CrystEngComm

Accepted Manuscript

ROYAL SOCIETY OF CHEMISTRY

www.rsc.org/crystengcomm

Journal Name

ARTICLE

Solid acetone structure dependence with pressure. New fibre textured thin film crystallographic structure studied by grazing-incidence X-ray diffraction.

Received 00th January 20xx,
Accepted 00th January 20xx

DOI: 10.1039/x0xx00000x

www.rsc.org/

P. Ferrer [a,b], I. da Silva [a,c], I. Puente-Orench [d,e*]

Recently, the development of miniaturized gas-sensing devices, particularly for toxic gas detection and for pollution monitoring, has been subject of intense research. A wide range of materials are available for acetone sensors, where the competition between the intermolecular forces and the molecule-substrate interactions play a crucial role. Despite this, the structural behaviour of acetone with temperature is still not fully understood. In this work, by varying the chemical vapour deposition rate on two different substrates at 120 K, two distinct acetone crystal structures were observed using grazing incidence X-ray diffraction. As well as a randomly oriented polycrystalline structure of the known orthorhombic phase, a new well-ordered fibre textured thin film structure with a related monoclinic structure was obtained. The phase obtained appears to be only dependent on vapour deposition pressures and not on the type of substrate, that is, the acetone crystal structure is controlled by the intermolecular forces, while substrate interactions do not seem to play any significant role. The significance of forming a fibre textured thin film structure in this manner is discussed.

INTRODUCTION

Gas sensors based on oxide semiconductors and metals have stood out from other gas detection methods and have received a tremendous attention during the last years. Such devices should allow for continuous concentration monitoring of particular gases in an environment, both in a quantitative and in a selective way.[1,2] The increasing demand of better gas sensors, with higher sensitivity and selectivity, has led to intense efforts to find more suitable materials with the required surface and bulk properties for applications in gas sensoring.

Different detection and quantification methodologies are applied, depending on the gaseous contaminants species to be detected in air (polluting gases).[3] Thus, understanding the interaction of the Volatile Organic Component (VOC) with surfaces, as well as the intermolecular structure, is imperative for the development of better gas sensors.

Most studies have focused on the design of novel material structures,[4] noble metal loading[5] and transition metal doping,[6] in an attempt to address increased sensibility, enhanced selectivity, outstanding reproducibility and long term stability[2] problems. The study of surface morphology, microstructure, crystalline size and composition of sensor supports has led to remarkably improved sensing performance.[7,8] However, only a small number of publications have explored the structure of the VOC itself under different environment (external) conditions.

In particular, in the last decade, there have been an increasing attention dedicated to the investigation of acetone-sensing materials and devices.[3,9,10] ZnO-based nanocrystals,[11,12] perovskite ABO_3 -type oxides,[13] SnO_2 –based nanocrystals[14,15] and two-dimensional WO_3 nanoplates[16] have been investigated as the sensitive materials for the detection of acetone vapour at various concentration levels. Given the interest that acetone gas sensors have raised, a thorough study of the intermolecular forces and surface interactions could provide new insights into this area.

Acetone, probably the most used polluting organic component, is the simplest member of the ketone family and it can be easily studied in gas, liquid or solid state. It is well established that non covalent interactions determine the

[a] SpLine-BM25 ICMM-CSIC, ESRF (European Synchrotron Radiation Facility), 6 rue Jules Horowitz, 38000, Grenoble, France..
[b] Diamond Light Source, Harwell Science and Innovation Campus, Chilton, Didcot OX11 0DE, UK.
[c] ISIS Facility, Rutherford Appleton Laboratory, Chilton, Oxfordshire OX11 0QX, UK.
[d] Universidad de Zaragoza, CSIC, Instituto de Ciencia de Materiales de Aragón, 50009, Zaragoza, Spain.
[e] Institut Laue-Langevin, BP 156, 38042, Grenoble Cedex 9, France.
† Present Address: F P.: Diamond Light Source, Harwell Science and Innovation Campus, Chilton, Didcot OX11 0DE, UK. I. dS.: ISIS Facility, Rutherford Appleton Laboratory, Chilton, Oxfordshire OX11 0QX, UK.
Corresponding author: puenteorench@ill.fr

function, dynamics and structure of biomolecules[17-23] and hydrogens bonds or carbonyl interactions are probably the most well-known examples of them. Depending on the conformation among carbon and oxygen atoms, there are three types of carbonyl-carbonyl interaction motifs,[24] namely i) perpendicular, ii) antiparallel and iii) parallel (Figure 1). Each acetone molecule is formed by two methyl groups, symmetrically connected to the C in a C=O bond, which makes it a good candidate for studying such interactions.

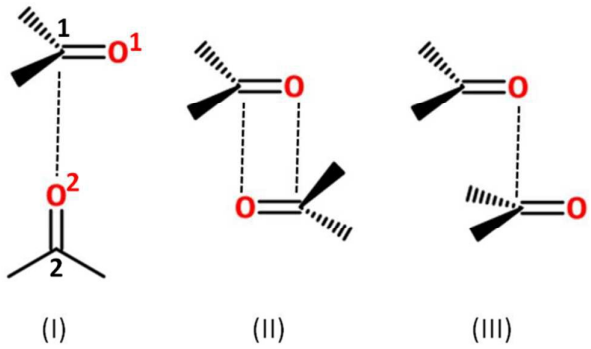

Figure 1. Perpendicular (I), antiparallel (II) and parallel (III) carbonyl type interactions motifs for dipolar carbonyl–carbonyl molecules[24]. Numbered C and O atoms are shown to facilitate the description of perpendicular interactions in Table 1.

Although acetone has been widely studied, mainly in the liquid or gaseous state, there are few published reports which deal with the phase transitions of solid acetone and they are not conclusive. Acetone crystallizes upon cooling beyond its melting point, of 179 K at ambient pressure. Felsing and Durban[25] studied the vapour pressure, density and latent heat of evaporation of acetone at low temperatures. Later on, in 1929, Kelly[26] studied the heat capacity of solid acetone and found a small heat capacity peak at 126 K, well below the melting point, which would suggest a phase transition. This question was not deeply studied until 1995 by Ibberson *et al*.,[27] when an anisotropic behaviour of the lattice parameters as a function of temperature was found and they concluded that this transition is not of the order-disorder type. They proposed, for the first time, that the most suitable crystal structure for solid acetone is orthorhombic. The seminal work of Allan *et al*.,[28] some years later, studied acetone crystals either prepared at room temperature and high pressure or by slowly cooling liquid acetone through the melting point at ambient pressure. They reported two stable orthorhombic crystalline structures, consisting of layers of molecules aligned along the *c*-axis. The arrangement of molecules inside those layers is described in terms of the three motifs presented above in Figure 1. Another C-centred orthorhombic metastable structure was found at a temperature of 165 K, however it decomposed after several hours. They also proposed that the anomaly of the heat capacity around 126 K is due to the strengthening of electrostatic contact among acetone molecules. The observed orientation for acetone molecules in the crystalline structures along the *c*-axis is not exclusive to the solid phase, as acetone molecules are oriented in the liquid state with one of the methyl groups pointing away from the bulk and the molecular plane perpendicular to the surface of the liquid.[29]

On the other hand, there are some studies dedicated to the investigation of acetone on flat metal or ice surfaces. Avery *et al*.[30,31] studied the interaction of acetone with Ru(001) and Pt(111) and they proposed two types of interactions: 1) end-on coordination, where the oxygen atom of acetone molecule interacts with the metal atoms of the surface, and 2) side-on configuration, where both the carbonyl C and O atoms are coordinated to the surface. Kusunoki *et al*.[32] studied the photodissociation of acetone multilayers adsorbed on Si(100); Takami *et al*.[33] dealt with the formation of SiC when exposing a Si(111) surface to acetone. Shin *et al.*[34] studied the structure of acetone under surface confinement and Almeida *et al.*[35] estimated the half-life of acetone ice in astrophysical environments. In all these works, crystallization of acetone underwent under non-conventional methods. That is, acetone was grown onto thin films, on top of a substrate, under certain conditions of pressure and temperature. However, up to our knowledge, structural studies of the crystallization of acetone thin films have not been reported, so far. It is known that different crystallization routes may yield new crystal structures and polymorphs, not previously observed.[36-41] Thus, for thin-films grown on surfaces the competing molecule-substrate and intermolecular forces may give rise to deformed, distorted or rotated structures which are not observed in the bulk.[42,43]
The aim of this work is to gain insight into the structure of crystalline acetone thin films, which could provide a better understanding of acetone gas sensors. Acetone crystals have been grown *in-situ* at 120 K in a special ultra-high vacuum (UHV) baby-chamber,[44] on Si(100) and Cu(110) substrates, at two pressures. Acetone crystals were studied by Grazing Incidence X-Ray Diffraction (GI-XRD),[45] taking advantage of the fact that the surface signal is maximized with respect to the bulk, to obtain information on the lateral and perpendicular atomic structure. To our knowledge, this is the first study which presents two-dimensional diffraction patterns of crystalline acetone. Moreover, the crystalline structure exhibited by the acetone differs depending on the dose rate, with a polycrystalline structure and a previously unreported fibre textured thin film structure being identified.

EXPERIMENTAL PROCEDURE

The X-ray diffraction experiments at grazing incidence angle (GI-XRD) were carried out on the six-circle diffractometer at the SpLine beamline (BM25B@ESRF, Grenoble, France).[46,47] The wavelength was fixed at 0.826 Å, with the maximum Q range explored of ~3 $Å^{-1}$ and a beam dimension of 0.3 x 0.3 mm^2. The incident angle was set to 0.2 and 0.5 degrees during data recording for Si(100) and Cu(110) substrates, respectively (Surface Preparation Laboratory - 99.999% purity and MATECK - 99.9999% purity, respectively). GI-XRD diffraction images during the crystallization process were collected with a 2D-

charge coupled device (Photonic Science CCD). The sample-detector distance was 250 mm and a good signal-to-noise ratio was obtained with exposure times of 30s. The camera produces a 250 mm x 125 mm 33 Mpixel resolution image with 32.8 µm pixel size and a final resolution of 3825 x 1912 pixels, after applying a 2x2 binning. The mesurements have been performed placing the long dimension of the detector perpendicular ,for Si(100), and parallel for Cu(110) with respect to the floor. The resulting images from the 2D-CCD detector were integrated using the XOP software.[48]

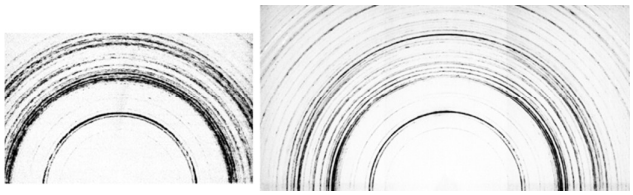

Figure 2. X ray pattern of the acetone deposited at 120 K, with a partial pressure above 10^{-4} mbar on Si(100) (left) and on Cu(110) (right).

Commercial acetone (CHROMASOLV® Plus, ≥99.9%, Sigma Aldrich) was directly used without further purification. Acetone crystals were grown *in situ* onto the surface of two different substrates, Si(100) and Cu(110). These substrates were placed inside of a dedicated UHV chamber, specially designed for GI-XRD studies.[44] The UHV chamber is equipped with a mass spectrometer and a capillary gas-inlet (0.9 mm ø) as the entry path for the acetone. Liquid acetone was contained in a small glass tube, separated from the main chamber by a controllable leak valve. The whole system was out gassed with a dry pump, purging the gas line several times. In order to enhance deposition of acetone onto the substrate, the capillary was placed about 10 mm from the substrates. The crystallization temperature was set to 120 K while the gas flowed through the leak valve into the chamber. The cold substrate surfaces were thus exposed to acetone vapour. The flow rate, during crystallization, was controlled by the pressure changes inside UHV chamber and the readings of the mass spectrometer.

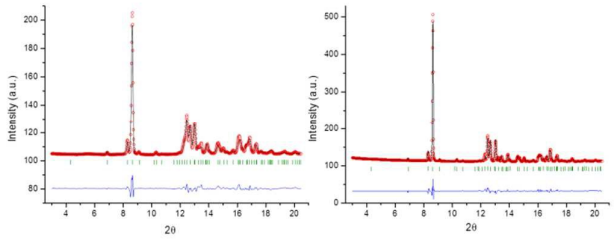

Figure 3. Rietveld refinement results, corresponding to Si(100) and Cu(110) substrates (left and right, respectively), showing the observed (red) and calculated (black) patterns. Difference is shown in blue and green tick marks indicate reflection positions.

The two substrates were first subjected to a cleaning process and, after that, their surfaces were checked by means of X-ray reflectivity. The Si(100) substrate was cleaned following Shiraki's method,[49] so an amorphous SiO_2 layer of about 2 nm was on top of the substrate, which was not removed by the cleaning process. The Cu(110) substrate was heated up to 500 °C, before cooling for acetone deposition, for removing surface impurities. In the case of the Cu(110), the reflectivity curve showed a clean and smooth surface.

RESULTS AND DISCUSSION

Following the deposition method described in the experimental part, we were able to study crystallized acetone. Due to the pressure and temperature of our experiment, acetone molecules, which enter in the UHV chamber in gaseous state, solidify when in contact with the cold surface of the substrate. Depending on the partial pressure in the UHV chamber during the deposition of the acetone vapour, two different crystalline structures develop. At pressures of around 10^{-4} mbar, acetone adopts a randomly oriented polycrystalline structure, whereas when depositing acetone at lower pressures, of about 10^{-7} mbar, it crystallizes in a previously unreported oriented fibre textured thin film structure. It is worth mentioning here that the lower the pressure of acetone vapour the lower the dose rate of deposition, while the higher the pressure the faster the deposition rate. Both structures are discussed below in detail.

Vapour pressure is the pressure at which the vapour of a substance is in thermodynamic equilibrium with its condensed phases. For acetone, it is known that it has a vapour pressure of 247mbar at room temperature.[50] This value changes with the temperature and the pressure of the environment. The empirical equation followed by the vapour pressure of acetone is:[25] $logP = -\frac{3981.28911}{T} + 27.676097 - 54.4585399 \times 10^{-3}T + 56.87851110^{-6}T^2$. Where P is in mbar and T is the temperature in K. At the temperature of the crystallization of our experiment (120 K), that is the temperature of the substrate, acetone's vapour pressure is 5.1 x 10^{-9} mbar. On the other hand, the partial pressures during deposition of acetone were 10^{-4} mbar, when a polycrystalline structure was obtained, and 10^{-7} mbar, when the fibre textured thin film structure arises. By following the above equation, these pressures correspond to temperatures of 152 K and 128 K, respectively. That is, for the case of the polycrystalline structure, the temperature of equilibrium between the gas and condensed phase (152 K) is well above the crystallization temperature. However, for the case of the fibre textured thin film structure the temperature of equilibrium (128 K) is closer to that of the crystallization experiment. This has a direct impact in the stability of the crystalline phases, being the fibre textured thin film more delicate of obtaining.

Polycrystalline structure

When depositing acetone molecules onto both substrates at 10^{-4}mbar, they crystallize in a randomly oriented crystalline structure. Figure 2 shows the 2-D diffraction patterns of acetone crystallized *in situ*, on top of both the substrates used in this study. One can observe well defined Debye-Scherrer

diffraction rings, which are the footprint of a polycrystalline structure. The intensity distribution along them is rather homogeneous, ruling out any significant preferred orientations of acetone crystals.

Using the available orthorhombic crystalline structure of acetone (CCDC number 118326),[28] we have successfully refined, by means of Rietveld method,[51] the isotropic crystalline structure grown at this dose rate (R_{wp} = 8.46% and 9.71% for Si(100) and Cu(110) substrates, respectively). The results of the Rietveld refinements are shown in Figure 3 and the obtained values of cell parameters, a = 8.84(2) Å, b = 7.94(2) Å and c = 21.92(6) Å for the case of Si(100) substrate and a = 8.819(3) Å, b = 7.971(3) Å and c = 21.96(1) Å, for the case of Cu(110) substrate, agree very well with the values obtained by Allan *et al.* (1999), using neutron diffraction (a = 8.873(3) Å, b = 8.000(4) Å and c = 22.027(7) Å).

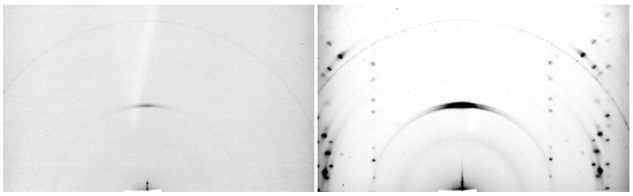

Figure 4. X ray patterns for the deposited acetone at 120 K on Si(100) under a partial pressure of 10^{-7} mbar after ~30 seconds (left) and 10 minutes (right). Polycrystalline Debye-Scherrer rings are due to the Be-window of the UHV chamber.

It is interesting to point out that in the experiments of Ibberson *et al.* (1995) and Allan *et al*. (1999) acetone powder was obtained at ambient pressure by cooling liquid acetone and grinding the obtained solid, in order to avoid preferred orientation effects. However, in the present experiment acetone is crystallized from its gaseous state in a random arrangement, getting the very same structure at different temperature and pressure conditions.

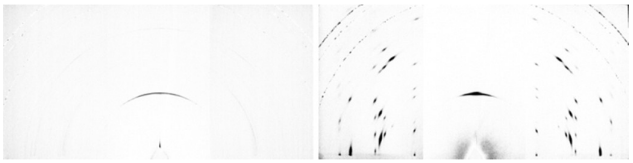

Figure 5. X ray patterns for the deposited acetone at 120 K on Cu(110) under a partial pressure of 10^{-7} mbar after ~30 seconds (left) and 10 minutes (right). Polycrystalline Debye-Scherrer rings are due to the Be-window of the UHV chamber.

Fibre textured thin film structure

We have shown that, at a partial pressure of 10^{-4} mbar in the UHV chamber, acetone crystallizes in a known orthorhombic crystalline structure. However, when the partial pressure of acetone during deposition at 120 K is 10^{-7} mbar, the crystalline structure obtained is completely different and, according to our knowledge, has not been reported before. Figures 4 and 5 (right) show the diffraction patterns of this novel structure phase when depositing acetone onto Si(100) and Cu(110), respectively. Here, instead of having diffraction rings, intense spots are found and, significantly, the diffraction pattern/image remains unaltered when the azimuthal angle is changed, that is, the sample is rotated around the surface normal. This fact clearly indicates that the obtained structure is a fibre textured one, in which the fibre axis is perpendicular to the substrate surface. Moreover, as with the polycrystalline structure previously presented, this new crystalline phase of acetone is found for both substrates.

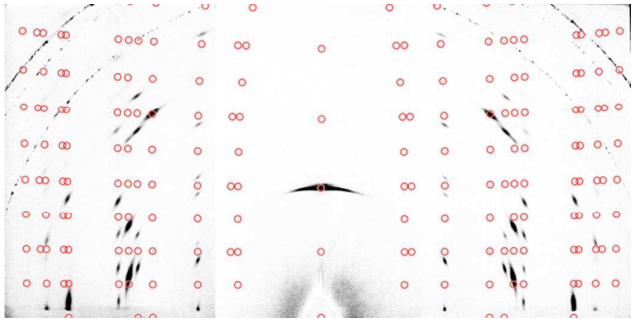

Figure 6. Calculated Bragg peak positions and X ray pattern of the orthorhombic acetone crystal cell. Polycrystalline Debye-Scherrer rings are due to the Be-window of the UHV chamber.

Throughout these experiments, this new highly oriented phase was observed several times. Low deposition dose rates of acetone promote the orientation of acetone crystals, under these specific pressure and temperature experimental conditions. A signal indicating that this fibre textured thin film structure is going to develop is that the diffraction patterns collected during the first minutes of acetone crystallization have a particular anisotropy (see left patterns of Figures 4 and 5). One can deduce that, when crystallizing acetone at temperatures and pressures close to those of equilibrium among its phases, acetone crystals do not grow onto the surface substrate with random orientations, but they rearrange in such a way that favours a specific crystallographic direction. There is little influence of the substrates on the observed preferred orientation, because the same structure arises on both Si(100) and Cu(110). By comparing the orthorhombic crystal cell of the polycrystalline phase, already solved, with the diffraction patterns obtained at 10^{-7}mbar, it could be suggested that the intense signal observed at the early deposition stages corresponds to the (004) reflection and, under these conditions, the crystal cells grow in a preferred direction along *c*-axis, that is parallel to the surface normal. Together with the intense oriented reflection, Debye-Scherrer rings can also be observed (see Figures 4 and 5), which are due to diffraction coming from the Beryllium window of the UHV chamber. After 10 minutes of deposition (Figures 4 and 5, right), new intense reflections appear quasi-parallel to the meridian, confirming that acetone crystals have continuously grew along the 00*l* direction.

Apart from rotating the substrate around the surface normal (azimuthal) axis (which yields the same diffraction pattern), the presence of a fibre textured thin film structure can be also confirmed by changing the angle between the incident X-ray beam and the fibre axis, which induces a shifting of the

diffraction spots along the vertical axis on the 2-D images obtained. Therefore, it is shown that, under the actual experimental conditions, the acetone crystal structure is oriented along the normal to the substrate surface, while the crystal cells can randomly rotate around this axis.

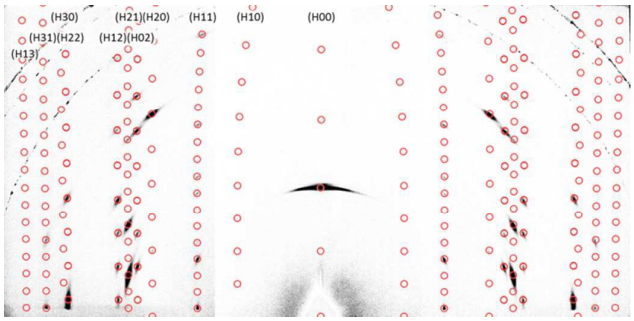

Figure 7. Calculated Bragg peak positions and X ray pattern of the monoclinic fibre acetone crystal cell. The Miller indexes for the different families of lattice planes along *h* are indicated. Polycrystalline Debye-Scherrer rings are due to the Be-window of the UHV chamber.

The subsequent question to answer now is: what is the actual crystalline structure and the arrangement of acetone molecules inside the crystal cell? It will be shown that this crystalline structure is different to that of its polycrystalline counterpart.

As stated previously, the intense reflection which appears at the early stages of deposition could, in principle, be associated with the (004) reflexion of the published orthorhombic structure of acetone, as it appears at an equivalent *d*-spacing. This would mean that the fibre textured thin film structure is, in fact, formed by acetone crystal cells with their *ab* planes parallel to the substrate and randomly rotating around the *c* axis. However, a two dimensional fibre diffraction pattern, which was calculated with FibreFix software[52] using this orthorhombic structure configuration, shows that the position of the experimental diffraction spots are not matched by the positions of the calculated ones (see Figure 6). This strongly suggests that an unknown crystal cell has been obtained.

In our quest to solve this new crystalline phase of acetone, we used a combination of simulation and refining softwares. Firstly, we searched for the suitable crystalline cell parameters which reproduce the obtained 2-D diffraction pattern. To do this, the angular positions of the diffraction spots were calculated using XOP program.[48] Note that, due to the low incident angle ($\propto$ = 0.2°) used to collect the data, double spots have been recorded for the case of Si(100) substrate (Figure 4, right). In the case of the Cu(110) substrate, where an incident angle of 0.5° has been used, clearer spots were recorded. Then, the position list was used for cell indexing, which was successfully performed with NTREOR program.[53] Thus, we have found that the oriented acetone reflections can be indexed with a monoclinic cell, with a = 22.268 Å, b = 8.671 Å, c = 7.993 Å and β = 95.10°. Comparing this result with the published acetone crystal structure, which is orthorhombic (space group *Pbca*) with a = 8.873 Å, b = 8.000 Å, and c = 22.027 Å, the result may point out that when acetone crystals grow normal to the substrate surface, the orthorhombic cell is distorted. The largest in-plane parameter has been reduced in 2.3% and the long axis (out-of-plane) has been elongated in 1.1%. Figure 7 shows all the allowed Bragg reflection positions, calculated with FibreFix software, corresponding to the indexed monoclinic crystal cell. The Miller indices for the different families of lattice planes along the *h* reciprocal space axis are also indicated for one half of the symmetric equivalent diffraction spots on the image. The space group used for the calculation was $P2_1/c$, which is the maximal monoclinic space group of *Pbca*. The calculated positions perfectly match the observed ones, demonstrating the accuracy of the new unit cell.

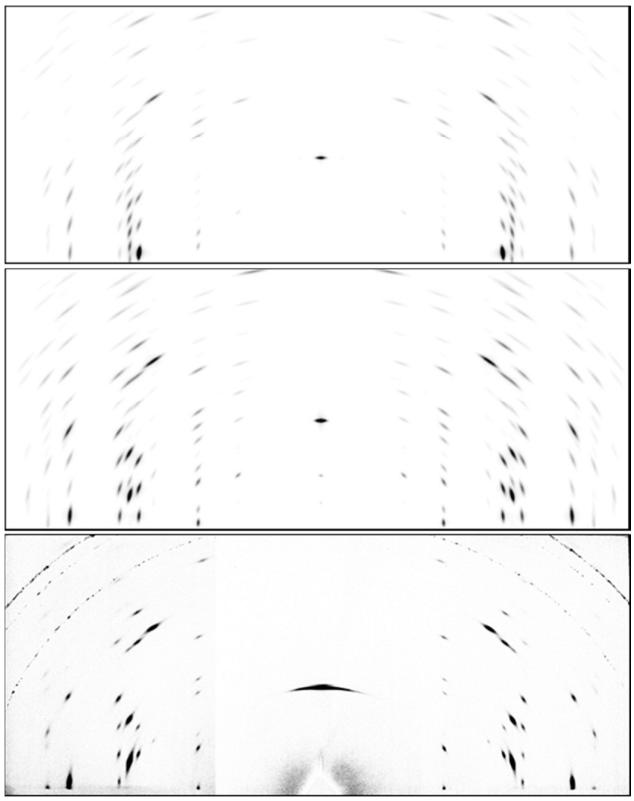

Figure 8. Diffraction pattern simulations for the case of monoclinic-transformed published acetone crystal structure (up) and fibre acetone crystal structure obtained by Monte-Carlo calculations (middle). The experimental diffraction pattern is shown at the bottom of the figure (Debye-Scherrer rings are due to the Be-window of the UHV chamber).

The next question to answer is if the actual modification on the cell parameters forces a new distribution of the molecules in the unit cell. To study the arrangement of acetone molecules, a 2-D diffraction image was simulated with the Anaelu program[54] using as input a transformed version of the published acetone structure. This structure has the same fractional coordinates of all the atoms of the orthorhombic cell, now referred to the monoclinic one. The output of this simulation can be seen on the upper image of Figure 8. The simulated pattern is quite different from the experimental one

(bottom image of Figure 8), which clearly indicates that there is not only a simple distortion of the cell, but it should also be a change in the atomic positions of the crystal structure.

In order to find out which is the new atomic arrangement, a Bragg intensity extraction from the diffraction pattern was performed with the FibreFix program, obtaining as a result a list of 82 *hkl*-intensity. This list was then used as input information in a Monte-Carlo calculation for crystal structure solving, which was performed using the Fox program.[55] Four crystallographically independent acetone molecules were used in the calculations; they were treated as rigid fragments; only their positions and orientations within the unit cell were optimized. The solution found by Fox[‡] was then used for a new fibre diffraction image simulation, yielding this time a pattern which reproduces very well the experimental one (see Figure 8, middle and bottom).

The published and experimentally found acetone crystal structures viewed along both the short axes have been schematically represented in Figure 9. As expected, the atoms allocated in the new fibre crystal structure present modifications from the published one. The new fibre textured crystal structure also consists on layers of acetone molecules, lying perpendicular to the long axis, in which the arrangement of the molecules alternates between antiparallel and perpendicular carbonyl-carbonyl interaction in the layers. The crystal structure is described in detail on the next paragraph.

Analysis of fibre textured thin film crystal structure.

We have seen that the acetone deposition rate on a surface has influenced the new crystal cell parameters; in this paragraph the new disposition of the molecules will be discussed. As mentioned above, the crystallographic axes found show a lack of symmetry in the structure, with a transformation from an orthorhombic to a monoclinic crystal cell. The orthorhombic acetone structure presents two crystallographically independent acetone molecules in the asymmetric unit; however, in the case of the fibre textured thin film structure studied in this work, four crystallographically independent molecules are required to completely describe the crystal structure, which is reflected into the carbonyl groups' interactions.

The orientations of the molecules in both orthorhombic polycrystalline and monoclinic fibre textured thin film structures can be described by two interactions: perpendicular (type I) and antiparallel (type II) (see Table 1). In the case of the fibre textured thin film structure, six motifs depend on the type of intermolecular interaction within the crystal structure (see Figure 10), while in the case of the bulk structure three are enough to describe it.

.

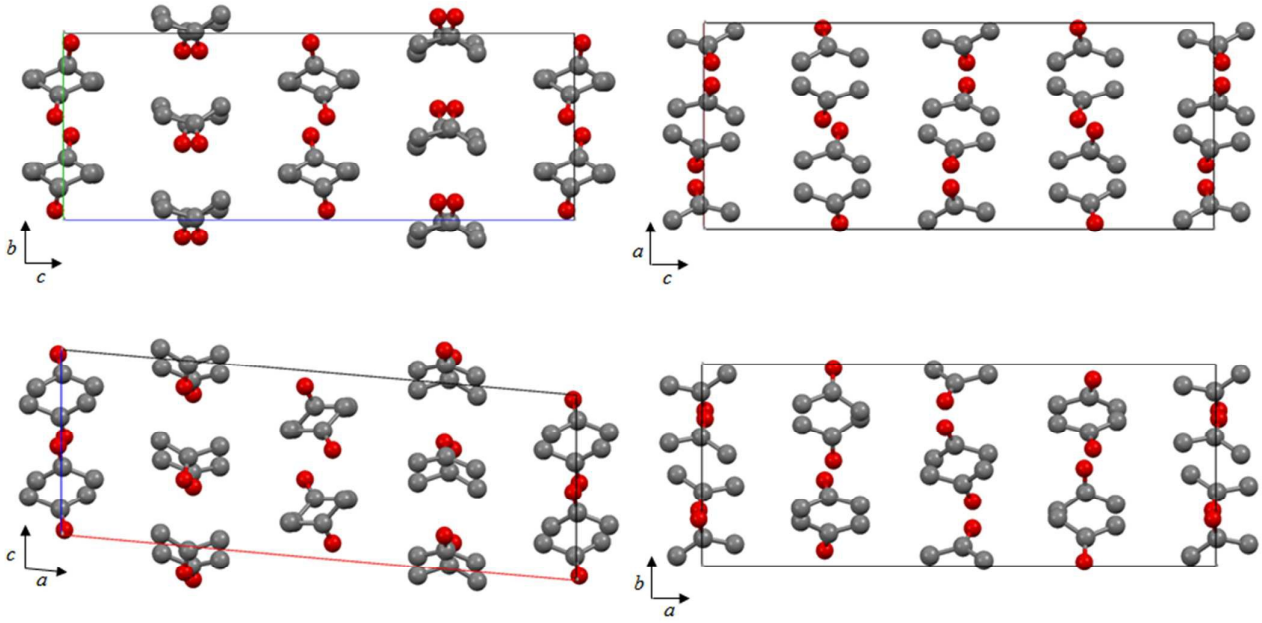

Figure 9 Schematic representation of the published acetone crystal structure (upper images) for comparison with the experimentally obtained structure (lower images).

Table 1. Intermolecular interactions, described for the polycrystalline and the new fibre-textured thin film acetone structures. Angles are described as: 1) C2-O2-C1, 2) O2-C1-O1, 3) C1-O1-C2 and 4) O1-C2-O2 (as shown in Figure 1).

	Molecules layer position along the long axis	Interaction type	Distance (Å)	Angle (degrees)
Orthorhombic polycrystalline acetone [Allan *et al*., 1999]	*c* ~ 0 and 0.5	Perpendicular type I	3.49	1: 167.49 2: 113.08 3: 56.15 4: 18.92
		Antiparallel type II	3.30	C-O-C: 84.81 O-C-O: 95.19
	c ~ 0.25	Perpendicular type I	3.46	1: 151.57 2:113.68 3: 59.27 4: 29.14
Monoclinic new fibre textured thin film acetone	*a* ~ 0	Perpendicular type I	3.32	1: 155.60 2: 116.61 3: 55.42 4: 39.31
		Antiparallel type II	3.42	C-O-C: 70.14 O-C-O: 109.86
	a ~ 0.25	Perpendicular type I	3.15	1: 149.73 2: 113.51 3: 60.36 4: 36.34
		Perpendicular type I	4.15	1: 164.23 2: 93.81 3: 75.82 4: 22.73
	a ~ 0.5	Perpendicular type I	3.71	1: 150.98 2: 102.81 3: 64.21 4: 25.77
		Antiparallel type II	3.29	C-O-C: 83.63 O-C-O: 96.37

Figure 10 shows the molecular dispositions for the different acetone layers, along the long axis (*c* for the orthorhombic and *a* for the monoclinic case, respectively). For the *c*, *a* ~ 0 layer, it can be observed that the molecular layer is shifted half a unit cell in both *b* and *c* directions respect to the orthorhombic structure, while just slight differences in the orientations of the arranged molecules of both structures can be seen, which present perpendicular and antiparallel carbonyl interactions motifs in an equivalent way. For the *c*, *a* ~ 0.25 layer, acetone molecules in the fibre textured thin film structure present a perpendicular carbonyl interaction motif, as in the case of the bulk structure. In the new structure, the interaction occurs between two crystallographically independent molecules (opposite to the case of the published structure where there is only one independent molecule); due to this fact, angles obtained for the perpendicular interaction results in a high distortion. Positions and orientations of the molecules are analogous on this layer for both structures. The main difference between both structures arises when comparing the molecule layers at *c*, *a* ~ 0.5. For the published structure this layer is symmetrically equivalent to the *c* ~ 0 layer, thanks to the *a* glide plane parallel to the *c* axis, while this is not valid for the fibre textured thin film structure. In the case of the fibre textured thin film structure, the layer shows an antiparallel interaction between the molecules as in the case of the bulk structure, but with the particularity that the whole layer has been displaced half a crystal cell in the *c*-axis direction from the expected position, and the orientation of the molecules is quite different from the orthorhombic case.

It is remarkable that the acetone has the same crystallization behaviour for both Si(100) and Cu(110) substrates, growing with the same preferred orientation along the *h*00 axis. The first monolayers are allocated with the *a* axis perpendicular to the surface. However, from our data we could not determine how the very first acetone molecular layer was bonding to the substrate. Taking into account how the acetone molecules are arranged in the crystal cell of the new fibre textured thin film structure, it could be deduced that they are bonded to the surface by the C atom from the methyl group and not by the lone pair of electrons that the oxygen atom presents. Thus, the acetone molecular configuration presents a C atom on the surface, bringing the O-C bond (carboxyl group) almost parallel to the surface.

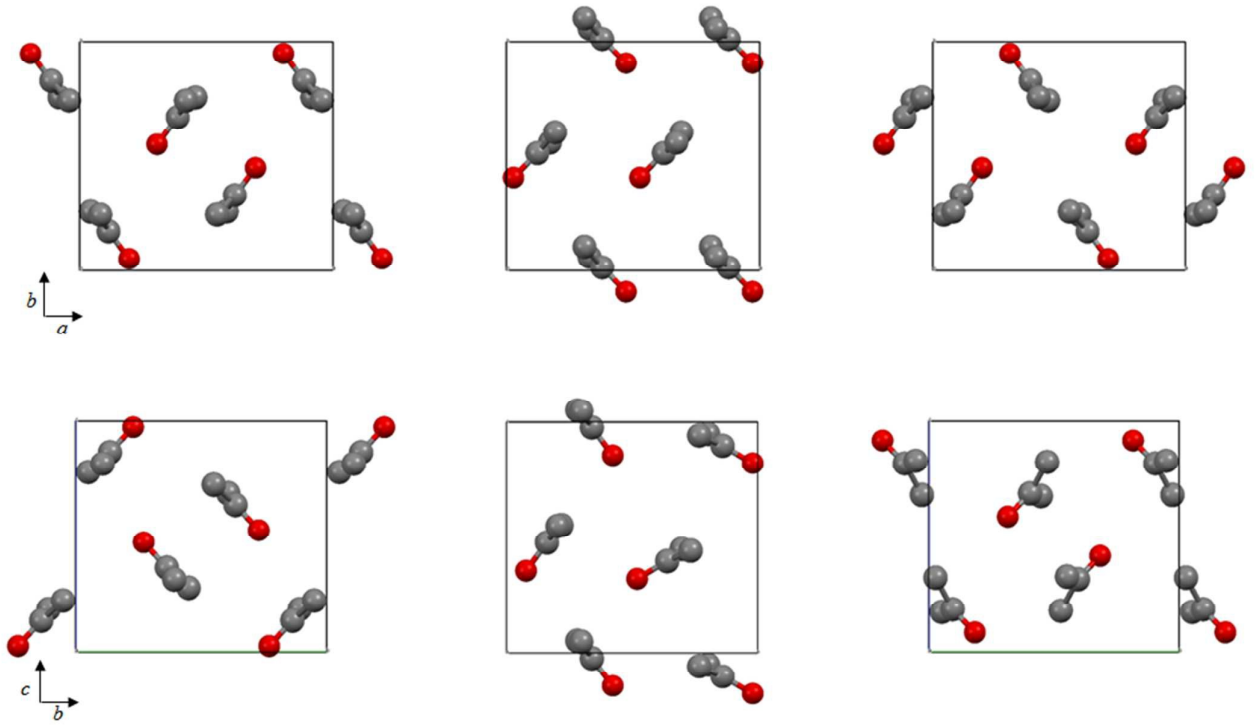

Figure 10 Three different layers of the acetone molecules viewed along the long axis (*c* and *a* for orthorhombic and monoclinic cases, respectively) at *c*, *a* ~ 0; *c*, *a* ~ 0.25 and *c*, *a* ~ 0.5 (left, centre and right images, respectively). Upper figures correspond to the published orthorhombic structure, while lower figures correspond to the monoclinic fibre textured thin film crystal structure. In each case, red and grey atoms correspond with O (oxygen) and C (carbon) atoms, respectively.

From the acetone molecule disposition, and taking into account that the experimental diffraction patterns are equivalent for both substrates, we can assert that there is no influence either from the degree of crystallinity or from the Si or Cu atoms of the substrates. We suggest that this behaviour is characteristic of the acetone molecules when they are deposited on a highly flat surface.

Conclusions

We have successfully crystallized acetone thin films directly from its vapour phase under UHV conditions at 120 K on two different substrates and studied them using GI-XRD. Depending on the dose rate of the deposition, two different crystalline structures have been found. At a pressure of 10^{-4} mbar, a non-oriented orthorhombic crystalline structure is obtained, where acetone molecules arrange in layers following perpendicular or anti-parallel motifs. However, at a pressure of 10^{-7} mbar, acetone crystals grow with a particular orientation with respect to the substrate surface, adopting a new monoclinic crystalline structure, where acetone molecules are also arranged in layers.

The crystal growth process of the new monoclinic structure proceeded via a self-preferential ordering of acetone crystal cells along the *h*00 axis.

This study provides new insights into the crystallisation of acetone thin films on surfaces. Bringing a better understanding of such physical processes could lead to the development of acetone gas sensors with enhanced performance characteristics such as increasing sensitivity. Importantly, our work demonstrates that the structure of fibre textured acetone thin films is controlled by the intermolecular forces and substrate interactions do not seem to play any significant role.

Acknowledgements

We thank the SpLine staff for their assistance in using beamline BM25B-SpLine. The financial support of the Consejo Superior de Investigaciones Científicas and Spanish Ministerio de Ciencia e Innovación (PI201060E013 and MAT2011-23758) is also acknowledged.

Notes and references

‡ CCDC 1494990 contains the supplementary crystallographic data for this paper. These data can be obtained free of charge from The Cambridge Crystallographic Data Centre via www.ccdc.cam.ac.uk/structures.

1 A. Mandeles and C. Christofides, Physics, Chemistry and Technology of Solid State Gas Sensor Devices. (John Wiley & Sons, Inc.), New York, 1993.
2 X. Zhou, B. Wang, H. Sun, C. Wang, P. Sun, X. Li, X. Hu and G. Lu, *Nanoscale,* 2016, **8**, 5446.
3 G. Eranna, B. C. Joshi, D. P. Runthala and R. P. Gupta, *Crit. Rev. Solid State Mater. Sci.*, 2004, **29**, 3-4, 111.
4 J. H. Lee, *Sens. Actuators, B.*, 2009, **140**, 319.
5 W. Shin, S. J. Choi, I. Lee, D. Y. Youn, C. O. Park, J. H. Lee, H. L. Tuller and I. D. Kim, *Adv. Funct. Mater.*, 2013, **23**, 2357-2367.
6 R. K. Mishra, A. Kushwaha and P. P. Sahay, *RSC Adv.*, 2014, **4**, 3904.
7 X. Zhou, Y. Xiao, M. Wang, P. Sun, F. M. Liu, X. S. Liang, X. W. Li and G. Y. Lu, *ACS Appl. Mater. Interfaces*, 2015, **7**, 8743.
8 C. Wang, X. Y. Cheng, X. Zhou, P. Sun and X. L. Hu, *ACS Appl. Mater. Interfaces*, 2014, **3**, 12031.
9 A. A. Zvyagin, A. V. Shaposhnik, S. V. Ryabtsev, D. A. Shaposhnik, A. A. Vasil'ev and I. N. Nazarenko, *J. Anal. Chem.*, 2010, **65**, 94.
10 B. Chen, Y. Yang, F. Zapata, G. Lin, G. Qian and E. B. Lobkovsky, *Advanced Materials*, 2007**, 19**, 13, 1693.
11 P. P. Sahay, *J. Mater. Sci.*, 2005**, 40**, 4383.
12 Y. Zeng, T. Zhang, M. X. Yuan, M. H. Kang, G. Y. Lu, R. Wang, H. T. Fan, Y. He and H. B. Yang, *Sens. Actuators B: Chem.*, 2009**, 143**, 93.
13 X. Liu, J. Hu, B. Cheng, H. Qin and M. Jiang, *Sens. Actuators B: Chem.*, 2008, **134**, 483.
14 J. Zhao, L. H. Huo, S. Gao, H. Zhao and J. G. Zhao, *Sens. Actuators B: Chem.*, 2006, **115**, 460.
15 L. Qin, J. Xu, X. Dong, Q. Pan, Z. Cheng, Q. Xiang and F. Li, *Nanotechnology*, 2008**, 19**, 185705.
16 D. Chen, X. Hou, T. Li, L. Yin, B. Fan, H. Wang, X. Li, H. Xu, H. Lu, R. Zhang and J. Sun, *Sensors and Actuators B*, 2011**, 153**, 373.
17 C B. Anfinsen, *Science*, 1973, **181**, 223.
18 K. J. Kamer, A. Choudhary and R. T. Raines, *J. Org. Chem.*, 2013, **78**, 5, 2099.
19 K A. Dill, *Biochemistry*, 1990, **29**, 7133.
20 A. Choudhary, D. Gandla, G. R. Krow and R. T. Raines, *J. Am. Chem. Soc.*, 2009, **131**, 21, 7244.
21 S. Y. Noskov, S. Bernèche and B. Roux, *Nature*, 2004, **431**, 830.
22 X. Xiu, N. L. Puskar, J. A. P. Shanata, H. A. Lester and D. A. Dougherty, *Nature*, 2009, **458**, 534.
23 Z. Han, T. Niu, J. Chang, X. Lei, M. Zhao, Q. Wang, W. Cheng, J. Wang, Y. Feng and J. Chai, *Nature*, 2010**, 464**, 1205.
24 F. H. Allen, C. A. Baalham, J. P. M. Lommerse and P. R. Raithby, *Acta Cryst. B*, 1998, **54**, 320.
25 W. A. Felsing and S. A. Durban, *J. Am. Chem. Soc.*, 1926, **48**, 11, 2885.
26 K. Kelley, *J. Am. Chem. Soc.*, 1929, **51**, 1145.
27 R. M. Ibberson, W. I. F. David, O. Yamamuro, Y. Miyoshi, T. Matsuo and H. Suga, *J. Phys. Chem.*, 1995, **99**, 14167.
28 D. R. Allan, S. J. Clark, R. M. Ibberson, S. Parsons, C. R. Pulhamd and L. Sawyer, *Chem. Commun.*, 1999, **751**.
29 Y. L. Yeh, C. Zhang, H. Held, A. M. Meel, X. Wei, S. H. Lin and Y. R. Shen, *Journal of Chemical Physics*, 2001, **114**, 4, 1837.
30 N. R. Avery, *Surface Science*, 1983, **125**, 771.
31 N. R. Avery, W. H. Weinberg, A. B. Anton and B. H. Toby, *Phys. Rev. Lett.*, 1983, **51**, 8, 682.
32 I. Kusunoki, M. Sakashita, T. Takaoka and H. Range, *Surface Science*, 1996, **357**, 693.
33 T. Takami, S. Ishidzuka, Y. Igari, H. Range and I. Kusunoki, *Thin solid Films*, 2000, **376**, 89.
34 S. Shin, H. Kan, J. S. Kim and H. Kang, *The Journal of Physical Chemistry B*, 2014, **118**, 13349.
35 G. C. Almeida, S. Pilling, D. P. P. Andrade, N. L. S. Castro, E. Mendoza, H. E. Boechat-Roberty and M. L. M. Rocco, *The Journal of Physical Chemistry C*, 2014, **118**, 6193.
36 D. S. Yutif and J. A. K. Howard, *Cryst. Eng. Comm.*, 2012, **14**, 2003.
37 D. Wiechert and D. Mootz, *Angew. Chem. Int. Ed.*, 1999, **38**, 1974.
38 A. D. Bond, *Chem. Commun.*, 2003, **250**.
39 A. R. Choudhury, K. Islam, M. T. Kirchner, G. Mehta and T. N. Guru Row, *J. Am. Chem. Soc.*, 2004, 126, **39**, 12274.
40 R. M. Ibberson, *Acta Cryst. B*, 2006, **62**, 592.
41 R. M. Ibberson, S. Parsons, D. R. Allan and A. M. T. Bell, *Acta Cryst. B*, 2008, **64**, 573.
42 S. M Johnston, A. Mulligan, V. Dhanak and M. Kadodwala, *Surface Science*, 2004, **548**, 5.
43 M. A. Vannice, W. Erley and H. Ibach, *Surface Science*, 1991, **254**, 1.
44 P. Ferrer, J. Rubio-Zuazo, C. Heyman, F. Esteban-Betegón and G. R. Castro, *J. Synchrotron Rad.*, 2013, **20**, 474.
45 G. Renaud, *Surface Science Reports*, 1998, **32**, 1.
46 G. R. Castro, *J. Synchrotron Rad.*, 1998, **5**, 657.
47 J. Rubio-Zuazo, P. Ferrer, A. López, A. Gutiérrez-León, I. da Silva and G. R. Castro, *Nucl. Instrum. Meth. A*, 2013, **716**, 2.
48 M. Sánchez del Río and R. J. Dejus, *Advances in Computational Methods for X-Ray Optics II, SPIE proceedings*, 2011, 814115.
49 A. Ishizaka and Y. Shiraki, *J. Electrochem. Soc.*, 1986, **133**, 666.
50 D. R. Lide, CRC Handbook of Chemistry and Physics. 84th Edition.
51 H. M. Rietveld, *J. Appl. Cryst.*, 1969, **2**, 65.
52 G. Rajkumar, H. A. AL-Khayat, F. Eakins, C. Knuppa and J. M. Squirea, *J. Appl. Cryst.*, 2007, **40**, 178.
53 A. Altomare, G. Campi, C. Cuocci, L. Eriksson, C. Giacovazzo, A. G. G. Moliterni, R. Rizzi and P. E. Werner, *J. Appl. Cryst.*, 2009, **42**, 768.
54 L. Fuentes-Montero, M. E. Montero-Cabrera and L. Fuentes-Cobas, *J. Appl. Cryst.*, 2011, **44**, 241.
55 V. Favre-Nicolin and R. Černý, *J. Appl. Cryst.*, 2002, **35**, 734.